Applied Nanoscience
https://doi.org/10.1007/s13204-018-0639-6

ORIGINAL ARTICLE

Impact of the titania nanostructure on charge transport and its application in hybrid solar cells

Alejandro Koffman-Frischknecht[1,4] · Fernando Gonzalez[1] · Juan Plá[1] · Ianina Violi[1] · Galo J. A. A. Soler-Illia[2] · M. Dolores Perez[1,3]

Received: 17 November 2017 / Accepted: 9 January 2018

Abstract

Porous titania films are widely studied in a number of optoelectronic applications due to its favorable optical and electronic characteristics. Mesoporous titania thin films (MTTFs) with tunable pore size, pore order, accessibility and crystallinity are of interest in electronic devices due to the potential for optimization of the desired characteristics for charge separation and carrier transport. In this work, several MTTFs were prepared by sol–gel chemistry with different structural properties tuned by post-synthesis thermal treatment. The effect of the structural properties (pore diameter, order and accessibility) on the electrical properties of the material was studied by films fabrication onto a transparent conducting electrode, ITO, such that it enables optoelectronic applications. The performance as photoanode was explored by the fabrication of hybrid polymer (P3HT): titania solar cells. Not only does structural properties affect polymer impregnation inside the titania pores as expected and hence impacts charge separation at the interface, but also the thermal treatment affects crystallinity and the films electronic properties. A more complete picture about the electronic properties of the different MTTFs prepared in this work was studied by mobility measurement by space charge limited current and impedance spectroscopy.

Keywords Mesoporous titania · Hybrid solar cells · Transport properties

Introduction

Porous titania thin films are widely studied in a number of applications, like photocatalysis (Al-Hamdi et al. 2017; Cao et al. 2014; Hoffmann et al. 1995; Schneider et al. 2014), sensors (Fujishima et al. 2008; Şennik et al. 2010; Zakrzewska 2004) and particularly in optoelectronic devices (Shakeel Ahmad et al. 2017; Wu et al. 2011). It is extensively used for solar cells (Abrusci et al. 2011; Bai et al. 2014; Coakley and McGehee 2003; Jafarzadeh et al. 2016; Rawolle et al. 2013; Wright and Uddin 2012) and is now thriving again due to its application in perovskite solar cells (Günes and Sariciftci 2008; Hwang et al. 2017; Zhang et al. 2016; Zuo et al. 2016). In those devices, the titania is mostly fabricated from a nanocrystalline titania paste that yields films with high porosity and thicknesses that can vary from a few hundred nanometers to microns. However, the accessible porosity, pore diameter and pore order are hard to control due to the nature of the fabrication method. Many efforts have been dedicated to the study of mesoporous titania thin films (MTTFs) to achieve tunable pore size, pore order, accessibility, and connectivity, as well

Electronic supplementary material The online version of this article (https://doi.org/10.1007/s13204-018-0639-6) contains supplementary material, which is available to authorized users.

✉ M. Dolores Perez
mdperez@tandar.cnea.gov.ar

Alejandro Koffman-Frischknecht
alejandro.koffman@probien.gob.ar

1 Departamento Energía Solar, GIyA-INN (Instituto de Nanociencias y Nanotecnologías), Centro Atómico Constituyentes, Comisión Nacional de Energía Atómica (CNEA), Av. General Paz 1499, 1650 San Martín, Provincia de Buenos Aires, Argentina

2 Instituto de Nanosistemas, UNSAM, 25 de Mayo y Francia, 1650 San Martín, Buenos Aires, Argentina

3 Escuela de Ciencia y Tecnología, Universidad Nacional de San Martín (UNSAM), 25 de Mayo y Francia, 1650 San Martín, Buenos Aires, Argentina

4 PROBIEN-Departamento de Electrotecnia, CONICET-Universidad Nacional del Comahue, Buenos Aires 1400, 8300 Neuquén, Argentina

Published online: 24 February 2018

as the crystallinity of the inorganic wall. These characteristics are highly relevant to understand the optimum use of MTTFs in advanced technologies (Carreon et al. 2007; Hartmann et al. 2010). For instance, photocatalysis is favored by the mesostructure order and pores accessibility and size, due to an improved molecular diffusion into the active surface centers. Nanocrystalline anatase titania is also desired since it offers the proper energetics (conduction band position and energy gap, Eg) for charge separation. The control of such properties is achieved through film post-synthesis thermal treatment where initial crystallite nucleation gives way to wall densification and crystallite growth as the temperature rises and therefore, define the mesostructure (Violi et al. 2012; Zhang et al. 2009). It has been well established that the nature of the substrate fully influences the rates of crystal growth and pore organization such that the development of ordered, highly porous and nanocrystalline MTTF on transparent conducting electrodes like ITO (indium tin oxide)-covered glass has been a challenge (Angelomé et al. 2007; Violi et al. 2012). A transparent substrate is needed for photovoltaic applications, since illumination needs to be carried out from the bottom of the MTTF that it also acts as an electrode for charge collection. In a previous work, we have comprehensively studied the effect of post-synthesis thermal treatment on the structural properties of titania layers in order to understand the annealing effect on parameters, such as mesostructure order; pore volume, size, accessibility and connectivity; and wall crystallinity (Violi et al. 2012). We observed the impact of these parameters on the photocatalytic performance of the titania, where surface effects dominate the photodegradation mechanism. However, it is still important to evaluate the titania structural characteristics on devices where charge is extracted from the materials, i.e., where photogenerated charges move through the bulk towards the electrodes for collection. This mechanism is an essential part of the functioning of solar cells and needs to be evaluated in order to identify whether those properties that were desired for photocatalysis are also favorable for photovoltaic (PV) applications.

In a typical optoelectronic application such as hybrid solar cell that employs porous titania and a semiconducting polymer, typically P3HT, there are several steps involved in the photovoltaic conversion mechanism where the nature of the photoanode is crucial. These include charge separation at the interface and charge collection at the electrode among other relevant optoelectronic processes. The presence of a highly porous inorganic material creates a tailored and stable interface that enhances charge separation. The porosity and pore dimensions will determine the titania surface area, and ordered and larger pores will provide a less truncated path for the holes and electrons to move through the material to reach the electrode. However, structural properties will not necessarily account for the behavior of the final device because the electronic characteristics of the materials play an important role in the performance of solar cells. Carrier mobility affects charge build-up and the recombination rates at the interface and in the bulk. Also, the materials electronic energetics will have a direct impact on the efficiency of charge separation at the interface. Whereas much effort is dedicated to the study of the materials structural properties, little is known about the mesoporous titania electronic properties and its dependence on the thermal post-synthesis.

In this report, we follow up a previous work where several MTTFs were fully characterized by diverse structural techniques (Violi et al. 2012). The titania films were fabricated onto ITO in contemplation of their use in optoelectronic applications. Here, we study the performance of the solar cells employing the different fabricated structures in an effort to relate the photoconversion efficiency of devices with the mesoporous structure of the MTTF. We first examine the polymer impregnation and its influence on the device performance. And then, in order to get a complete picture of the use of MTTFs in electronic devices, we study the electronic properties of the materials by mobility calculation with the space charge limited current method, and impedance spectroscopy.

Experimental

Titania films were deposited onto ITO-covered glass substrates by dip coating from ethanolic solutions containing a titania precursor, $TiCl_4$ (Sigma Aldrich). A full description of the preparation process is presented in a previous work by Violi et al. 2012. Briefly, a solution with molar ratio of 1Ti:40EtOH:10H_2O is used for the dense layer and for the porous layer, a triblock copolymer Pluronic F127® (Sigma) is added as a pore directing agent to yield a final ratio of 1Ti:40EtOH:10H_2O:5 × 10^{-3}F127. ITO glass substrates were purchased from Delta Technologies Ltd. (R_{sh} = 5–15Ω). Six types of samples were prepared combining dense and mesoporous titania layers. Non-porous titania (named D for "dense") was prepared by dip coating at a constant withdrawal rate of 1 mm s^{-1} under controlled relative humidity (RH) of 20%. After deposition, the films were stabilized for 30 min at 60 °C and finally calcined at 350 °C (1°C min^{-1}) during 2 h (D3). Further thermal treatment on specific films involved exposure to 500 °C for 60 min (D5). The F127-templated titania mesoporous layers (labeled M for "mesoporous") were prepared by dip coating (withdrawal rate of 2 mm s^{-1}) under controlled relative humidity of 35%. After coating, films were placed in a 50% RH chamber for 24 h, and followed by 24 h at 60 °C, 24 h at 130 °C and a final calcination at 350 °C for 2 h (thermal ramp of 1 °C min^{-1}) (M3). Some films were further treated at 550 °C for 30 min with a "flash" type treatment (M5). All

the thermal treatments were done in a furnace (INDEF, Córdoba, Argentina) under a still air atmosphere. Bilayers were prepared by deposition of the dense layer and consolidation at both temperatures (D3 and D5); and successive deposition of the mesoporous followed by the previously mentioned heat treatment in order to achieve all combinations (D3M3, D3M5, D5M3 and D5M5). Samples without dense layers were also prepared, namely M3 and M5. All samples were cut in order to remove the naked ITO region (where the sample hangs for dipping) and also to remove the bottom zone where titania accumulates due to capillarity.

Prior to the organic material deposition, samples were further cleaned in an ethanolic bath for 30 min and then dried up in an oven at 130 °C for 10 min. To promote pores degassing, samples were submerged in toluene overnight. P3HT was used as-purchased (Rieke-Metals) and dissolved in toluene (10 mg mL^{-1}). Titania films were removed from the overnight toluene bath and placed directly in the spin coater to prevent ambient water to adsorb onto the titania surface. The polymeric solution was deposited onto the film with 60 s rest period to promote infiltration of the organic solution into the pores, prior to spinning at 3000 rpm for 1 min. Next, the samples were annealed at 200 °C for 5 min to eliminate the solvent and allow a deeper penetration of the polymer.

Consequent P3HT depositions were performed in ×1, ×2, ×3, ×5 and ×7 cycles on sample D3M5 in order to optimize the solar cell performance. Each cycle involves spin coating + annealing with a toluene flush prior to the following P3HT deposition in order to remove the top polymeric layer that could block empty pores from further impregnation. The last deposition cycle is not toluene cleaned to provide for a top hole transporting layer (HTL). PV device fabrication was finished by thermal evaporation of about 150 nm of the metallic contact, alternatively Ag and Au, in a vacuum chamber at $P_{background} = 1 \times 10^{-5}$ torr through a shadow mask. Solar cell areas were 7.85×10^{-3} cm^2.

J–V measurements were carried out with a Keithley 2602 source meter unit and a solar simulator consisting of a Xenon lamp and an AM 1.5 filter. 1 sun intensity was calibrated with an InGaP solar cell provided by the IES (Instituto de Energía Solar, Universidad Politécnica de Madrid) due to the similar spectral responsivity.

ITO sheet resistance was measured with a 4-Point Probe resistivity system from Signatone Corp. The measurement was performed onto the substrates with finished titania films prior to cutting for device processing. Probes were situated onto the naked ITO region that is left unexposed during the dipping process. Top and cross-section scanning electron microscopy (SEM) images were obtained with Carl Zeiss NTS-SUPRA 40SEM.

Mobilities calculated by the Space Charge Limited Current (SCLC) were obtained using a Keithley 2602 source. High voltages are needed in order to reach space charge regime so as to apply the Mott–Gurney theory for trap-free materials, by applying the equation ($J = (\frac{9}{8})_0 \mu (\frac{V^2}{L^3})$) where the dependence of the current density, J, with the applied voltage, V, follows a quadratic behavior. Here, μ is the mobility, ε_0 and ε are the vacuum and material permittivity, respectively, and L is the titania film thickness. We use $\varepsilon = 60$, according to previously reported values (Stamate 2003). Devices with the structure ITO/TiO_2/Au were fabricated for space charge measurements. Au metal contact was chosen for this experiment instead of Ag because the resulting devices were more robust and afforded higher applied voltages before breaking down.

Impedance measurements were acquired with a Metrohm Autolab 302N potentiostat, applying a sinusoidal signal with amplitude of 0.1 V, and a frequency sweep from 1 Hz to 1 MHz with a logarithmic spacing. The amplitude was defined to avoid polarization of the sample and the frequency range was the largest possible.

Results and discussion

Solar cells with the structure ITO/TiO_2:P3HT/Metal, as shown in Fig. 1, were fabricated in order to establish the effect of the titania structure on the photovoltaic performance. Here, the dense titania layer behaves as an electron transporting layer (ETL) and the top P3HT layer is desired to work as a hole transporting layer (HTL). Both Au and Ag metals were evaluated as contacts because of their optimum work function for hybrid photovoltaic devices. Ag contacts resulted in better device performance than Au, probably because the latter chemically reacts with the thiophene (see Supplementary material) (Nambu et al. 2003). To ensure full infiltration of the polymer inside the titania pores and provide for a top hole conducting layer of optimum thickness, several spin coating + annealing cycles of the polymer were performed and fully characterized. The intensity of the UV–Vis absorbance spectra increases with successive spin coating depositions (see Supplementary material), indicating an incremental polymer amount upon successive

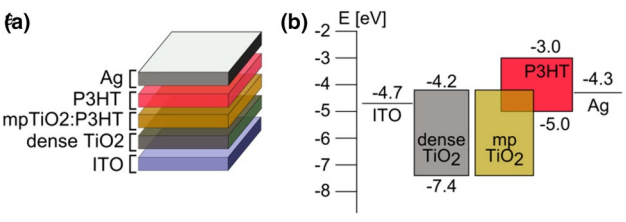

Fig. 1 **a** Schematic representation of inverted device structure Ag/P3HT(HTL)/P3HT:TiO_2/TiO2(ETL)/ITO layers from the top down. **b** Energy diagram of each layer corresponding to the device structure

cycles, inside the titania pores or overflowing as a top layer. We must note, as detailed earlier, that after each spin coating–annealing cycle, the top layer is cleaned with a toluene flush except for the last cycle. This is done in order to ensure that the polymer fibers depositing on top of the titania do not block empty pores and allow further filling of empty pore spaces on the next spin coating cycle.

From the SEM images, top and side view (Fig. 2), we can observe the effect of successive impregnation cycles of the polymer over the titania films. The side-view images reveal that the polymer penetrates inside the pores and overflows the titania surface when pores are filled, as observed for 5 cycles (×5) where a thick layer of P3HT is visible on top of the MTTF (~ 150 nm). The top-view images also reveal this sequence by exhibiting the titania surface coverage. For ×1 cycle, we observe islands of P3HT fibers and nude titania surface as it appears that the polymer mostly penetrates inside the pores and little remains on the top layer acting as HTL. The titania pores are almost fully covered for ×3 and a compact polymer layer in the form of fiber is present for ×5 sample as the HTL becomes thicker.

The solar cells *J–V* performance for the different polymer cycles with Ag contact was measured and shown in Fig. 3. For ×1 polymer deposition + annealing cycle, we observe a reduced open circuit voltage, V_{OC}, and similar photocurrent to the ×2 cycles device. The lower V_{OC} is a consequence of the incomplete coverage of the HTL on the titania surface as observed in Fig. 2; the top P3HT layer inhomogeneity allows immediate contact of the Ag electrode with the titania, producing recombination sites that reduce the V_{OC}. On the other hand, the short circuit current density, J_{SC}, reaches a maximum for ×3 to drop again for ×5 and ×7 deposits. This type of behavior is typically observed for an increase in the hole transporting layer thickness. As P3HT is accommodated inside the titania pores, the photocurrent rises due to the increase of the absorbed light as reflected in

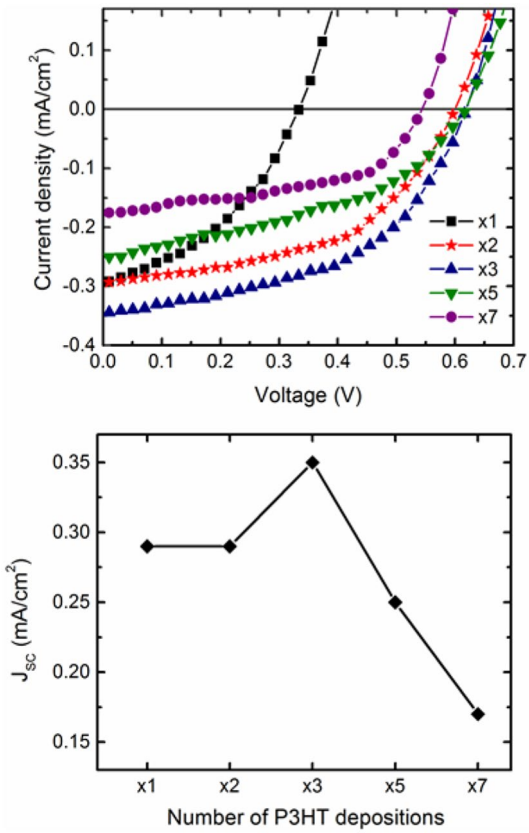

Fig. 3 *J–V* curves (top) and J_{SC} dependence (bottom) of devices with different P3HT depositions

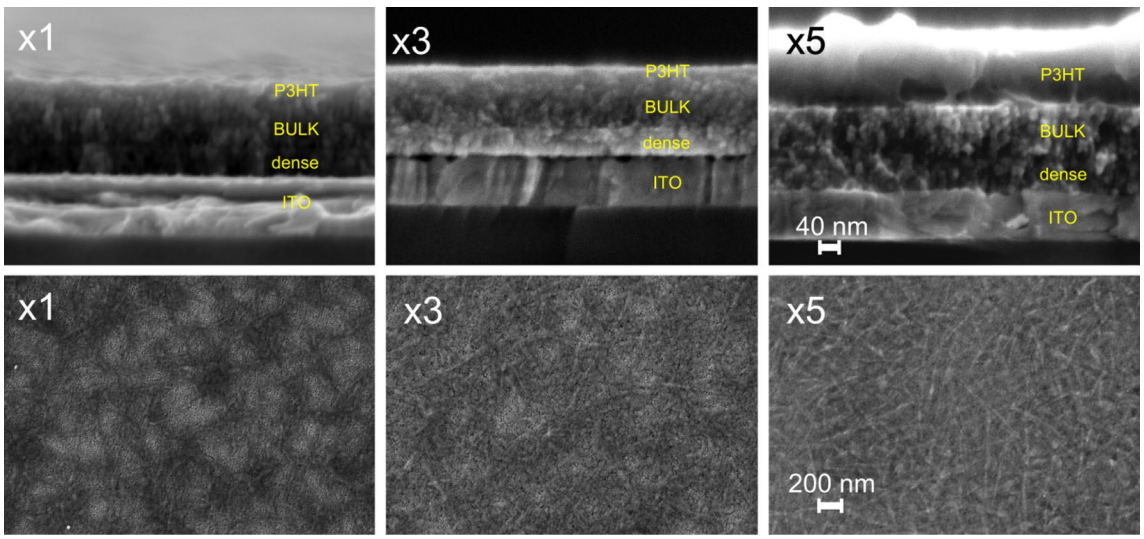

Fig. 2 Cross-section (top) and top-view (bottom) SEM image of samples with ×1, ×3 and ×5 P3HT depositions

the absorbance spectra (Supplementary material), more photons absorbed near the interface means more photogenerated charges. But if the polymer builds up as a thick top layer, the photocurrent decreases because the excitons generated far from the interface may easily recombine before reaching the titania/P3HT interface. Even though the P3HT is on the back side of the device, it will have an effect on the back light reflected at the metallic contact because the optical field is no longer optimized for the TiO_2:P3HT active region. The device optical field profile can be modeled according to the transfer matrix optical model for multilayer stacks developed by Burkhard et al. (2010). For 540 nm (P3HT maximum absorption wavelength), we can observe a maximum optical field at the active TiO_2:P3HT bulk region for the ×3 sample, whereas for the thicker ×5 P3HT layer (ca. 150 nm from the SEM image) the light intensity in the photoactive bulk is much lower. Even though the J_{SC} calculation through this model assumes an internal quantum efficiency, IQE = 100%, we calculated a 21% lower J_{SC} for the ×5 compared to the ×3 (see Fig. 4).

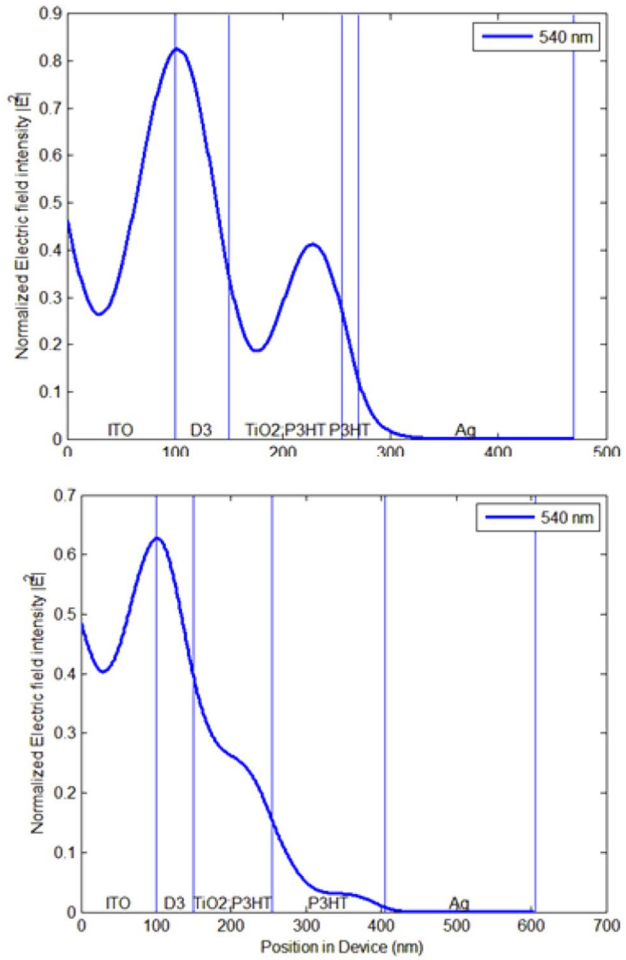

Fig. 4 Simulation of optical field profiles of 540 nm light for devices with 50 nm (×3) (top) and 150 nm (×5) (bottom) P3HT overlayers

To study the effect of the titania mesostructure on the device performance, we made devices using three cycles of P3HT deposits + annealing for optimum performance. We employed different titania samples prepared by combination of thermal conditions that were fully characterized in a previous work by Violi et al. 2012. Figure 5 shows the *J*–*V* characteristic curves under illumination for devices of the structures: ITO/My:P3HT/P3HT/Ag and ITO/Dx/My:P3HT/P3HT/Ag. The poor performance of the D5My devices first strikes attention, in particular because the D5M5 has been shown to perform best photocatalytically (Violi et al. 2012), whereas here it shows zero photocurrent generation with very poor diode behavior. D5M3 also has a very poor performance with high series resistance. See Table 1 for the device parameters. On the other hand, the D3My devices show the best performance. D3M5 presents higher photocurrent than D3M3 as expected from the significant difference in the accessible pore volume, 29.1% for D3M3 and 49.2% for D3M5 according to reference Violi et al. 2012. A higher pore accessibility favors increased amount of P3HT inside the titania pores that photogenerate higher current. The pore diameter (PD) is also tied to the accessible pore volume (PD:6.7 nm for D3M3 and PD:9.0 nm for D3M5) (Violi et al. 2012) because the pore size increases due to a sintering effect from wall surface reconstruction; for smaller pore size, titania walls are thicker and viceversa. It has also been shown that heat treatment also accounts for the titania walls crystallinity, D3M5 titania shows polycrystallinity as observed by SAED (selected area electron diffraction), whereas D3M3 titania appears amorphous (Violi et al. 2012). The thicker and amorphous walls of the D3M3 films are responsible for the larger series resistance of the corresponding solar cell that also impacts on the V_{OC} and the fill factor (FF) values.

Devices that employ both mesoporous titania structures in direct contact with ITO, without the dense layer (M3 and

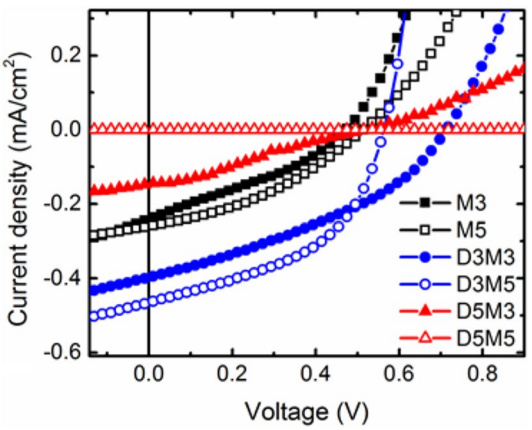

Fig. 5 *J*–*V* curves of M3, M5, D3M3, D3M5, D5M3 and D5M5 devices with ×3 P3HT impregnation

Table 1 Electrical output parameters: efficiency (η), fill factor (FF), short circuit current (J_{SC}) and open circuit voltage (V_{OC}); series resistance (R_s) and shunt resistance (R_p) of devices with titanias: M3, M5, D3M3, D3M5, D5M3, D5M5

Device	η (%)	FF (%)	J_{SC} (Ma cm^{-2})	V_{OC} (V)	R_s (Ω cm^2)	R_p (10^3 Ω cm^2)	ITO R_{sh} ($\Omega/\square$)
M3	0.04	32.67	0.24	0.47	49.54	3.16	68
M5	0.05	36.75	0.26	0.51	112.42	3.91	75
D3M3	0.10	36.57	0.40	0.71	76.73	3.98	70
D3M5	0.12	47.57	0.47	0.56	25.79	3.63	88
D5M3	0.02	26.37	0.16	0.52	1995.26	7.94	74
D5M5	–	–	–	–	–	–	60

M5), perform similarly and rather poorly. The dense layer has a twofold purpose: it behaves as an electron transport layer that prevents direct contact of the polymer with the ITO electrode hence impeding recombination, and it also works as a structuring agent for the mesoporous structure. Both M3 and M5 have no long range pore order and no crystallinity is observed from the titania walls, as opposed to DxM3 that shows *Im3m* pore order and DxM5 with both grid-like pore structure and wall crystallinity. These two effects combined (i.e., P3HT exciton recombination at the ITO surface and lack of pore order and titania crystallinity) results in high series resistance and poor J_{SC}. This is compatible with the earlier photodegradation studies where M3 and M5 structures had a mediocre performance compared to those structures with a dense layer as a structuring layer (Violi et al. 2012). From all the above, it is evident that some materials features are desired to improve solar cell performance, such as pore diameter, accessible porosity and titania walls crystallinity. However, structural properties are not enough to predict if materials will have optimum photovoltaic performance as evidenced by the lack of photocurrent and poor performance of the solar cells fabricated with the D5M3 and D5M5 titanias, respectively. For D5My, it appears that the extensive heat treatment to the dense layer modifies energetics such that the titania layer becomes a blocking layer for electron extraction, whereas it does not affect the mesoporous layer attributes that yield optimum photocatalysis as was shown earlier (Violi et al. 2012).

The ITO substrate sheet resistance (R_{sh}) was measured for all samples (Table 1) in order to assess changes of the underlying substrate conductivity due to the heat treatment that could influence the device final performance. The R_{sh} are within 60–80$\Omega/\square$, definitely higher than the untreated ITO (5–15$\Omega/\square$ as purchased), as expected according to the previous reported literature that found that post-synthesis annealing affects the conductivity of the ITO due to changes in the microstructure (Chen et al. 2014). The detriment of the ITO conductivity could eventually have a negative impact on the device performance but it should result in a similar effect for all samples given that the R_{sh} are comparable.

The electron transport properties of thin films were characterized by the space charge limited current (SCLC) method. Mobilities were extracted by fitting the steady state *J–V* curve in the trap free region in forward bias according to the Mott–Gurney equation (Mott and Gurney 1948). In Table 2, we present the calculated mobility values. Please refer to Supplementary material for the *J–V* data curves and the fitting method. The higher mobility for the D3M5 sample is in conformity with the solar cells observed best efficiency. The other titania samples portray similar mobilities, with D5M5 sample being the lowest. In general, they all lie within previously reported values for porous titania of 10^{-6} to 10^{-3} cm^2 v^{-1} s^{-1} (Aduda et al. 2004; Crossland et al. 2013; Dittrich et al. 1998).

Table 2 SCLC mobilities for the different titanias

Sample	μ (10^{-4} cm^2 V^{-1} s^{-1})
M3	1.5
M5	1.2
D3M3	1.2
D3M5	2.3
D5M3	1.2
D5M5	0.85

Measurement of impedance spectroscopy allows the understanding of the different MTTF structures from the electrical point of view and relates the structural characteristics with an equivalent electronic circuit. Devices in the form ITO/DxMy/Ag and ITO/My/Ag were studied and the frequency response analyser (FRA) signals of the complex impedance $Z(\omega) = Z'(\omega) + IZ''(\omega)$ [where $Z'(\omega)$ and $Z''(\omega)$ are the real and imaginary part of the impedance, respectively], are depicted in Fig. 6a. The resulting impedance for all samples can be grouped into two distinctive responses according to the mesoporous layer thermal treatment. M5 and DxM5 samples show overall higher impedance than M3 and DxM3 titanias. All samples can be modeled by the equivalent circuit shown in Fig. 6b. The thin dense layer does not present an important contribution to the impedance included in the R_s. All fitted parameters are presented in Table 3.

The R_S agrees well with the expected resistance arising from the ITO to the contact probe, taking into account an

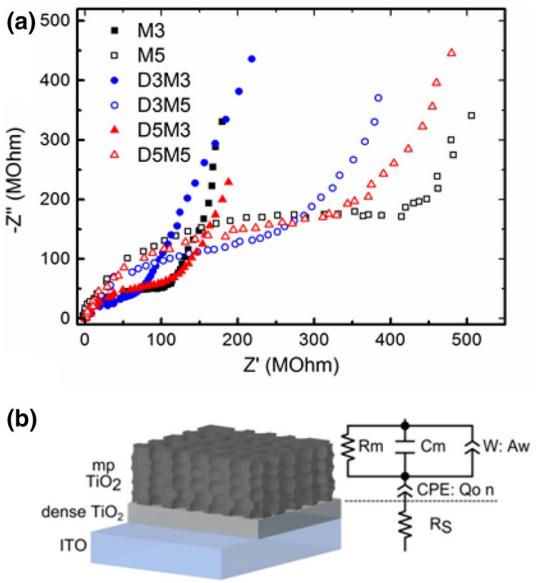

Fig. 6 **a** Impedance measurements, $Z'(\omega)$ vs. $Z''(\omega)$ for all titania samples. **b** Depiction of the equivalent circuit used for fitting

ITO sheet resistance of ~70 Ω/□ after heat treatment and the geometrical disposition of contacts and probes, the R_S calculated values would range between 300 and 2400 Ω. The capacitance values for the mesoporous layers (Cm) are all very similar, as corresponds to capacitors of similar thickness. On the other hand, the resistances found for the mesoporous layers (R_m) treated at 500 °C are generally higher than for those treated at lower temperatures. This effect may be a result of higher resistances arising from thinner titania walls and higher crystallite size with larger grain boundaries, observed for samples exposed at higher temperatures. A Warburg element is included in the equivalent circuit to account for moving charges other than electrons, e.g., ions, such that it follows the equation: $(Z_W = \frac{A_w}{\sqrt{\omega}}(1-i))$.

The Warburg component may be originated by the diffusion resulting from the adsorbed water within the mesopore surface given the highly hydrophilic nature of the titania surface. A lower A_w corresponds to increased diffusion according to the dependence $(A_w \propto \frac{1}{\sqrt{D}})$ where D is the diffusion coefficient. Remarkably, samples where the mesoporous layer was exposed to the same temperatures yield similar A_w values: 1.43, 2.48 and 1.86×10^{-9} Ω $s^{-1/2}$ for M5, D3M5 and D5M5, respectively, and 3.41, 3.62 and 3.41×10^{-9} Ω $s^{-1/2}$ for M3, D3M3 and D5M3, respectively. The generally lower A_w for M5 and DxM5 samples is in agreement with the reportedly larger pore diameters and accessible porous volume that would favor diffusion (Violi et al. 2012). More experiments are underway intended to study the impedance under different ambient humidity that will assess more clearly how the water contents affect the Warburg component.

A constant phase element (CPE) is also included in the equivalent circuit in order to account for the impedance behavior at lower frequencies, where $(Z_{CPE} = \frac{1}{Q_0}(\frac{1}{i\omega})^n)$. The fitted Q_0 and n constants are also presented in Table 3. We understand that the CPE describes the transport of charges through the titania interfaces to the subjacent layers. Given that the n values are close to 1, the CPE resembles a capacitor behavior. Samples with a dense layer include two interfaces (ITO/*D* and *D*/*M*) that reflects in higher CPE (lower Q_0), compared to My samples with a single interface and higher Q_0.

Conclusions

Considering the ample application of mesoporous titania thin films in a diversity of optoelectronic devices, it is most desired to understand how the MTTFs transport and extract charges. We have studied, from an electrical point of view, the introduction of a dense titania layer and posterior heat treatment on sol–gel prepared titanias onto ITO substrate. We observed that the structure in terms of pore size and accessibility most influences polymer impregnation in hybrid solar cells such that larger pores and higher accessible volume produce more efficient cells due to the increased amount of polymer within the bulk heterojunction. However, structural properties are not enough to determine if materials will have optimum photovoltaic performance, as evidenced by the poor performance of the solar cell fabricated with the D5M5 titania. This material had the best

Table 3 Fitted parameters for the equivalent circuit components (see Fig. 6b)

Sample	R_s (Ω)	R_m (MΩ)	C_m (pf)	A_w (10^{-9} Ω $s^{-1/2}$)	Q_0 (10^{-9} Ω^{-1} s^n)	n
M5	289	519	601	1.43	40.1	0.85
D3M5	692	369	660	2.48	33.7	0.86
D5M5	623	478	517	1.86	30.4	0.88
M3	342	140	500	3.41	37.2	0.87
D3M3	402	80.9	500	3.62	21.0	0.86
D5M3	583	146	562	3.41	26.4	0.81

reported photocatalytic performance, according to an earlier report, but the worst photovoltaic conversion. While photocatalysis is only a surface effect, in photovoltaics carriers need to migrate through the bulk material and reach the electrode with no trapping or recombination. The carrier mobility shows a slender dependence on the titania structural parameters, with D3M5 presenting a higher mobility, consistent with a better performance of the solar cells. From the impedance measurements, we were able to describe the equivalent electrical circuit for the different titania films. We observe that the component parameters are mostly dominated by the heat treatment of the mesoporous material and little information can be extracted on the effect of the dense layer on the mesoporous titania.

Acknowledgements The authors are indebted to M. C. Marchi (CMA-UBA) for the SEM measurements and the Nanochemistry group at CNEA for the titania films preparation facility. J. Plá, G. J. A. A. Soler-Illia and M. Dolores Perez are permanent researchers at Consejo Nacional de Investigaciones Científicas y Técnicas (CONICET). A. Koffman-Frischknecht, F. Gonzalez and I. Violi are supported by CONICET fellowships. We thank IES-UPM for the calibrated reference sensor.

Funding This work was supported by CNEA, ANPCyT (Grant PICT 1027-2013) and FUNINTEC-UNSAM (Grant INTERING 2016).

References

Abrusci A et al (2011) Facile infiltration of semiconducting polymer into mesoporous electrodes for hybrid solar cells. Energy Environ Sci 4:3051–3058. https://doi.org/10.1039/c1ee01135a

Aduda BO, Ravirajan P, Choy KL, Nelson J (2004) Effect of morphology on electron drift mobility in porous TiO_2. Int J Photoenergy 6:141–147. https://doi.org/10.1155/s1110662x04000170

Al-Hamdi AM, Rinner U, Sillanpää M (2017) Tin dioxide as a photocatalyst for water treatment: a review. Process Saf Environ Prot 107:190–205. https://doi.org/10.1016/j.psep.2017.01.022

Angelomé PC, Andrini L, Calvo ME, Requejo FG, Bilmes SA, Soler-Illia GJAA (2007) Mesoporous anatase TiO_2 films: use of Ti K XANES for the quantification of the nanocrystalline character and substrate effects in the photocatalysis behavior. J Phys Chem C 111:10886–10893. https://doi.org/10.1021/jp069020z

Bai Y, Mora-Seró I, De Angelis F, Bisquert J, Wang P (2014) Titanium dioxide nanomaterials for photovoltaic applications. Chem Rev 114:10095–10130. https://doi.org/10.1021/cr400606n

Burkhard GF, Hoke ET, McGehee MD (2010) Accounting for interference, scattering, and electrode absorption to make accurate internal quantum efficiency measurements in organic and other thin solar cells. Adv Mater 22:3293–3297. https://doi.org/10.1002/adma.201000883

Cao L, Chen D, Li W, Caruso RA (2014) Hierarchically porous titania networks with tunable anatase: rutile ratios and their enhanced photocatalytic activities. ACS Appl Mater Interfaces 6:13129–13137. https://doi.org/10.1021/am502990r

Carreon MA, Choi SY, Mamak M, Chopra N, Ozin GA (2007) Pore architecture affects photocatalytic activity of periodic mesoporous nanocrystalline anatase thin films. J Mater Chem 17:82–89

Chen Y, Jiang H, Jiang S, Liu X, Zhang W, Zhang Q (2014) Influence of annealing temperature on the microstructure and electrical properties of indium tin oxide thin films. Acta Metall Sin 27:368–372. https://doi.org/10.1007/s40195-014-0059-x

Coakley KM, McGehee MD (2003) Photovoltaic cells made from conjugated polymers infiltrated into mesoporous titania. Appl Phys Lett 83:3380–3382

Crossland EJW, Noel N, Sivaram V, Leijtens T, Alexander-Webber JA, Snaith HJ (2013) Mesoporous TiO_2 single crystals delivering enhanced mobility and optoelectronic device performance. Nature 495:215–219. https://doi.org/10.1038/nature11936

Dittrich T, Lebedev EA, Weidmann J (1998) Electron drift mobility in porous TiO_2 (anatase). Phys, Status Solidi A, p 165

Fujishima A, Zhang X, Tryk DA (2008) TiO_2 photocatalysis and related surface phenomena. Surf Sci Rep 63:515–582. https://doi.org/10.1016/j.surfrep.2008.10.001

Günes S, Sariciftci NS (2008) Hybrid solar cells. Inorg Chim Acta 361:581–588

Hartmann P, Lee D-K, Smarsly BM, Janek J (2010) Mesoporous TiO_2: comparison of classical sol–gel and nanoparticle based photoelectrodes for the water splitting reaction. ACS Nano 4:3147–3154. https://doi.org/10.1021/nn1004765

Hoffmann MR, Martin ST, Choi W, Bahnemann DW (1995) Environmental applications of semiconductor photocatalysis. Chem Rev 95:69–96

Hwang T, Lee S, Kim J, Kim C, Shin B, Park B (2017) Tailoring the mesoscopic TiO_2 layer: concomitant parameters for enabling high-performance perovskite solar cells. Nanoscale Res Lett. https://doi.org/10.1186/s11671-016-1809-7

Jafarzadeh M, Sipaut CS, Dayou J, Mansa RF (2016) Recent progresses in solar cells: insight into hollow micro/nano-structures. Renew Sustain Energy Rev 64:543–568. https://doi.org/10.1016/j.rser.2016.06.028

Mott NF, Gurney RW (1948) Electronic processes in ionic crystals. Clarendon Press, Oxford

Nambu A, Kondoh H, Nakai I, Amemiya K, Ohta T (2003) Film growth and X-ray induced chemical reactions of thiophene adsorbed on Au(111). Surf Sci 530:101–110. https://doi.org/10.1016/S0039-6028(03)00383-2

Rawolle M et al (2013) Infiltration of polymer hole-conductor into mesoporous titania structures for solid-state dye-sensitized solar cells. ACS Appl Mater Interfaces 5:719–729. https://doi.org/10.1021/am302255c

Schneider J, Matsuoka M, Takeuchi M, Zhang J, Horiuchi Y, Anpo M, Bahnemann DW (2014) Understanding TiO_2 photocatalysis: mechanisms and materials. Chem Rev 114:9919–9986. https://doi.org/10.1021/cr5001892

Şennik E, Çolak Z, Kilinç N, Öztürk ZZ (2010) Synthesis of highly-ordered TiO_2 nanotubes for a hydrogen sensor. Int J Hydrog Energy 35:4420–4427. https://doi.org/10.1016/j.ijhydene.2010.01.100

Shakeel Ahmad M, Pandey AK, Abd Rahim N (2017) Advancements in the development of TiO_2 photoanodes and its fabrication methods for dye sensitized solar cell (DSSC) applications. A review. Renew Sustain Energy Rev 77:89–108. https://doi.org/10.1016/j.rser.2017.03.129

Stamate MD (2003) On the dielectric properties of dc magnetron TiO_2 thin films. Appl Surf Sci 218:317–322. https://doi.org/10.1016/s0169-4332(03)00624-x

Violi IL, Perez MD, Fuertes MC, Soler-Illia GJAA (2012) Highly ordered, accessible and nanocrystalline mesoporous TiO_2 thin films on transparent conductive substrates. ACS Appl Mater Interfaces 4:4320–4330. https://doi.org/10.1021/am300990p

Wright M, Uddin A (2012) Organic–inorganic hybrid solar cells: a comparative review. Sol Environ Mater Sol Cells 107:87–111. https://doi.org/10.1016/j.solmat.2012.07.006

Wu CH, Li H, Fong HH, Pozdin VA, Estroff LA, Malliaras GG (2011) Room-temperature preparation of crystalline TiO_2 thin films and their applications in polymer/TiO_2 hybrid optoelectronic devices. Org Electron 12:1073–1079. https://doi.org/10.1016/j.orgel.2011.03.004

Zakrzewska K (2004) Gas sensing mechanism of TiO_2-based thin films. Vacuum 74:335–338. https://doi.org/10.1016/j.vacuum.2003.12.152

Zhang Y, Xie Z, Wang J (2009) Supramolecular-templated thick mesoporous titania films for dye-sensitized solar cells: effect of morphology on performance. ACS Appl Mater Interfaces 1:2789–2795

Zhang C, Luo Y, Chen X, Ou-Yang W, Chen Y, Sun Z, Huang S (2016) Influence of different TiO_2 blocking films on the photovoltaic performance of perovskite solar cells. Appl Surf Sci 388:82–88. https://doi.org/10.1016/j.apsusc.2016.03.093

Zuo C, Bolink HJ, Han H, Huang J, Cahen D, Ding L (2016) Advances in perovskite solar cells. Adv Sci 3:1500324. https://doi.org/10.1002/advs.201500324